Revised structural phase transitions in the archetype $KMnF_3$ perovskite crystal

Joanna Kapusta
Institute of Physics, University of Silesia, Uniwersytecka 4, 40-007 Katowice, Poland

Philippe Daniel*
Laboratoire de Physique de l'Etat Condensé, UPRES A CNRS No. 6087, Université du Maine, Avenue O. Messiaen, 72085 Le Mans Cedex 9, France

Alicja Ratuszna
Institute of Physics, University of Silesia, Uniwersytecka 4, 40-007 Katowice, Poland

(Received 17 February 1998; revised manuscript received 14 December 1998)

Reinvestigation of the structural and vibrational properties of the typical perovskite $KMnF_3$, exhibiting two antiferrodistortive structural phase transitions, was performed using x-ray powder diffraction and Raman spectroscopy in the range between 30 and 300 K. The x-ray-diffraction work has unambiguously shown that a monoclinic distortion ($a^-b^+c^-$ tilt system $P2_1/m$ space group) is observed at low temperature below $T_{C2}=91$ K. This result corresponds with the Raman temperature study which shows that this transition, in spite of its first-order character, can be associated with a group-subgroup relation between tetragonal and monoclinic symmetries. Additionally, existence of a large structural disorder far above the cubic to tetragonal transition ($T_{C1}=186$ K) is suggested by the two following experimental indications: (i) persistence of hard modes of the tetragonal phase in the cubic symmetry, and (ii) existence of Raman broad bands in normally inactive ideal cubic phase, which are interpreted by the folding of the whole phonons branches of the cubic Brillouin zone. This last observation allows us to follow the evolution of the cubic R'_{15} soft mode versus temperature, *based only on the Raman-scattering data*, in full agreement with previous inelastic neutron data. The results of Raman investigations into $KMnF_3$ are discussed in more general framework of structural disorder in perovskite systems which exhibit anisotropic correlation between octahedra. [S0163-1829(99)00522-6]

INTRODUCTION

Over the past three decades, structural phase transitions (SPT) have been extensively studied in crystals and the AMX_3 perovskite structures were one of the largest classes of samples investigated. This family is remarkable as it can readily evidence a great variety of structural instabilities from antiferrodistortive to ferroelectric and antiferroelectric ones. The antiferrodistortive transitions give rise from the ideal cubic symmetry to a lower symmetry, tetragonal or trigonal, when the temperature is reduced which results generally from instabilities of a low-energy phonon branch located at the Brillouin-zone corner of the cubic structure. These SPT can be usually described by the rotation of MX_6 octahedra around one of the major fourfold cubic axes, which causes that the distorted phase has a double unit cell as compared to the cubic phase, since the unstable mode responsible for the phase transition consists of alternating antiphase rotations of the MX_6 octahedra.

The perovskite $SrTiO_3$ (Ref. 1) was one of the most studied compounds corresponding to these phase transition mechanisms, where the soft-mode picture was first discussed in detail by Fleury, Scott, and Worlock[2] in the light of a Raman-scattering investigation. In this framework, the fluoroperovskite $KMnF_3$ has also appeared for a long time as an interesting crystal candidate (actually the first structural paper by Klassens, Zalm, and Huysman[3] devoted to this sample dates from 1953) since it undergoes a typical sequence for phase transitions in perovskite systems:[4–10] cubic→tetragonal→orthorhombic or monoclinic. The first transition, which is slightly of the first order, occurs at around $T_{c1}=186$ K and corresponds to the softening of the R'_{15} zone-boundary mode located at the $R(0.5,0.5,0.5)$ point of the reciprocal space. The high-temperature cubic space group O_h^1 ($Pm3m$-$a^0a^0a^0$ tilt system according to Glazer's labeling[11]) becomes tetragonal $D_{4h}^{18}(14/mcm)$ with the tetragonal c axis developing around the [001] cubic axis. This new symmetry can be symbolized by the tilt system $a^0a^0c^-$ where the $-$ superscript designates antiphase tilts around the main cubic axes (while the $+$ superscripts are used for the in-phase tilts of the octahedra). According to the literature[5,12–14] this transition is followed at lower temperatures by one additional transition at $T_{C2}=91$ K, claimed either with a first-order character[12] or with a second-order character.[14] This transition is associated with the softening of phonons which have the M_2 symmetry [zone-boundary mode located at the $M(0.5,0,0.5)$ point of the reciprocal space]. The structure of a low-temperature phase and the mechanism of this 91 K phase transformation have been the subject of contradictory studies for a long time (see, for instance, the discussion of Gibaud *et al.*[10] and Ratuszna and co-workers[15,16]), however, no definitive answer has been obtained. The hysteresis of several degrees appearing around this low-temperature transition was very often attributed to additional transformation while the investigation of the 91 K transition was enhanced by an additional magnetic transition at $T_{C3}=88$ K associated with the appearance of an antiferro

TABLE I. Irreducible representations associated with the motions of the three different atoms in $KMnF_3$. Low-temperature calculations are performed according to two proposed symmetries in the literature. It should be noted that this work concludes to the $P2_1/m$ monoclinic symmetry below $T_{C2}=91$ K.

Cubic phase-$Pm3m(O_h^1)$	Tetragonal phase-$I4/mcm(D_{4h}^{18})$
$\Gamma_K=F_{1u}$	$\Gamma_K=B_{2g}\oplus E_g\oplus A_{2u}\oplus E_u$
$\Gamma_{Mn}=F_{1u}$	$\Gamma_{Mn}=A_{1u}\oplus A_{2u}\oplus 2E_u$
$\Gamma_F=2F_{1u}\oplus F_u$	$\Gamma_F=A_{1g}\oplus 2A_{2g}\oplus B_{1g}\oplus B_{2g}\oplus 2E_g$ $\oplus 2A_{2u}\oplus B_{1u}\oplus 3E_u$
$\Gamma_{Total}=4F_{1u}\oplus F_{2u}$	$\Gamma_{Total}=A_{1g}\oplus 2A_{2g}\oplus B_{1g}\oplus 2B_{2g}\oplus 3E_g$ $\oplus A_{1u}\oplus 4A_{2u}\oplus B_{1u}\oplus 6E_u$
Γ_{Raman}—no Raman lines	$\Gamma_{Raman}=A_{1g}\oplus B_{1g}\oplus 2B_{2g}\oplus 3E_g$
Low-temperature phase	
Orthorhombic phase-*Pnma* (D_{2h}^{16})	Monoclinic phase-$P2_1/m$ (C_{2h}^2)
$\Gamma_K=2A_g\oplus B_{1g}\oplus 2B_{2g}\oplus B_{3g}\oplus A_u$ $\oplus 2B_{1u}\oplus B_{2u}\oplus 2B_{3u}$	$\Gamma_K=4A_g\oplus 2B_g\oplus 2A_u\oplus 4B_u$
$\Gamma_{Mn}=3A_u\oplus 3B_{1u}\oplus 3B2_u\oplus 3B_{3u}$	$\Gamma_{Mn}=6A_u\oplus 6B_u$
$\Gamma_F=5A_g\oplus 4B_{1g}\oplus 5B_{2g}\oplus 4B_{3g}\oplus 4A_u$ $\oplus 5B_{1u}\oplus 4B_{2u}\oplus 5B_{3u}$	$\Gamma_F=10A_g\oplus 8B_g\oplus 8A_u\oplus 10B_u$
$\Gamma_{Total}=7A_g\oplus 5B_{1g}7B_{2g}\oplus 5B_{3g}$ $\oplus 8A_u\oplus 10B_{1u}\oplus 8B_{2u}\oplus 10B_{3u}$	$\Gamma_{Total}=14A_g\oplus 10B_g\oplus 16A_u\oplus 20B_u$
$\Gamma_{Raman}=7A_g\oplus 5B_{1g}\oplus 7B_{2g}\oplus 5B_{3g}$	$\Gamma_{Raman}=14A_g\oplus 10B_g$

TABLE II. Parameters of the rigid-ion model and calculated zone-boundary eigenfrequencies in the ideal cubic perovskite phase of $KMnF_3$. Calculated frequencies are given in cm^{-1}.

Set of parameters of the rigid-ion model:
$A_{K\text{-}F}=6.43$ c.u. $=10.08$ N/m $\quad B_{K\text{-}F}=-0.64$ c.u. $=-1.00$ N/m
$A_{Mn\text{-}F}=44.21$ c.u. $=69.32$ N/m $\quad B_{Mn\text{-}F}=-4.19$ c.u. $=-6.57$ N/m
$A_{F\text{-}F}=8.18$ c.u. $=12.82$ N/m $\quad B_{F\text{-}F}=-0.82$ c.u. $=-1.28$ N/m
$Z_K^*=0.406 \quad Z_{Mn}^*=0.959 \quad Z_F^*=-0.455$

$\Gamma(0, 0, 0)$
$4F_{1U}: 0(L+T); 117.8(L+T); 201.0^{(2)}(T) 261.2^{(1)}(L); 400.2^{(2)}(T) 410.1^{(1)}(L)$
$F_{2U}: 156.5^{(3)}$

$R(0.5, 0.5, 0.5)$
$R'_{15}: 23.1^{(3)}; 2R'_{25}: 106.7^{(3)} 265.1^{(3)}, R_{15}: 186.2^{(3)}; R_{12}: 317.0^{(2)} R_1: 448.5^{(1)}$

$M(0.5, 0, 0.5)$
$M_2: 24.1^{(1)}; M'_2: 100.3^{(1)} 388.3^{(1)}; M'_5: 103.1^{(2)} 187.3^{(2)} 203.7^{(2)}; M'_3: 113.1^{(1)};$
$M_5: 176.0^{(2)}; M_4: 265.9^{(1)}; M_3: 317.1^{(1)}; M_1: 413.1^{(1)}$

$X(0, 0.5, 0)$
$X'_5: 78.5^{(2)} 177.5^{(2)} 394.0^{(2)}; X_5: 98.2^{(2)} 185.9^{(2)}; X_1: 126.8^{(1)} 373.8^{(1)};$
$X'_4: 160.8^{(1)}; X'_2: 183.3^{(1)} 251.5^{(1)}$

magnetic ordering.[8] Finally, the most probable sequence for phase transition can be summarized as follows using Glazer's classification:

$$\begin{array}{ccccccc} & T_{C1}=186\,\mathrm{K} & & T_{C2}=91\,\mathrm{K} & & & \\ a^0a^0a^0 & \Rightarrow & a^0a^0c^- & \Rightarrow & a^-b^+a^- & \text{or} & a^-b^+c^- \\ \text{cubic} & & \text{tetragonal} & & \text{orthorhombic} & & \text{monoclinic} \\ Pm3m & & I4/mcm & & Pnma & & P2_1/m. \end{array}$$

Popkov, Eremenko, and Fomin[17] investigated the 186 K cubic to tetragonal phase transition in $KMnF_3$ using Raman scattering and performed assignment of tetragonal lines. This work was followed by the major studies of Lockwood and Torrie,[18,19] the results of which confirmed the tetragonal symmetry adopted by this compound below 186 K and evidenced the appearance of two soft modes of E_g and A_{1g} symmetries coming from the R'_{15} cubic mode, associated with a displacive mechanism. Hard Raman modes, which are not directly involved in the transition, were also studied[20] and were interpreted in terms of precursor order parameter near the transition by Bruce, Taylor, and Murray.[21] Moreover, the magnetic transition was also studied by Raman scattering[22] with analysis of the two-magnon mode occurring together with the antiferromagnetic ordering.

So, why is it interesting to reinvestigate the archetype of this crystal from a structural and vibrational point of view? (i) Because, as previously underlined, the low-temperature structure of this compound with the associated phase transition mechanism is still a subject of controversy. Moreover, no Raman study has been fully performed and interpreted based on group theory analysis in low-temperature phase, despite the fact that Raman scattering could constitute an adapted probe to remove partially the structural ambiguities. (ii) The origin of Raman intensity which exists in the ideal cubic perovskite phase where no mode is expected was revealed by Lockwood and Torrie[18] but it was not fully explained and therefore needs additional studies. (iii) Furthermore, the disorder close to the tetragonal-cubic transition, predicted by different theoretical models[23,24] and recently identified by x-ray absorption fine structure (XAFS) experiments by Rechav *et al.*,[25] Yacoby and Stern (see, for example, Refs. 26 and 27) in ferroelectric oxygen perovskites ($PbTiO_3$, $BaTiO_3$, $SrTiO_3$) or Rousseau *et al.*[28] in $RbCaF_3$ (inelastic neutron scattering) seems to be also interesting to approach it in this type of perovskite.

In this paper, we report the results of an x-ray-diffraction study at low temperature as well as a Raman-scattering investigation into $KMnF_3$ in the range from 30–300 K; the assignment of the Raman lines is performed on the basis of a full group theory analysis. Special attention is paid to low-temperature phase and to unusual Raman activity in the ideal cubic perovskite symmetry.

EXPERIMENTAL METHOD

$KMnF_3$ crystal was grown, in a dry inert atmosphere using a modified Bridgmann-Stockbarger method[29] from high purity starting products and using and adopted temperature protocol. Transparent pink, very good optical quality crystals could be extracted from the crucible. A sample of dimension of about 0.5 cm^3 was cut and orientated by the x-ray Laüe method along fourfold cubic axes.

Powder x-ray-diffraction data were collected on a Siemens D5000 diffractometer. The filtered CuK_α radiation ($\lambda = 1.540\,56$ Å) was selected and ϑ/ϑ scans were recorded in a 18°–100° 2ϑ range with a step of 0.02°. At low temperature ($T = 12$ K) the experiment was performed in a HTT4 (Anthon Paar Physica) camera working in the close cycling system.

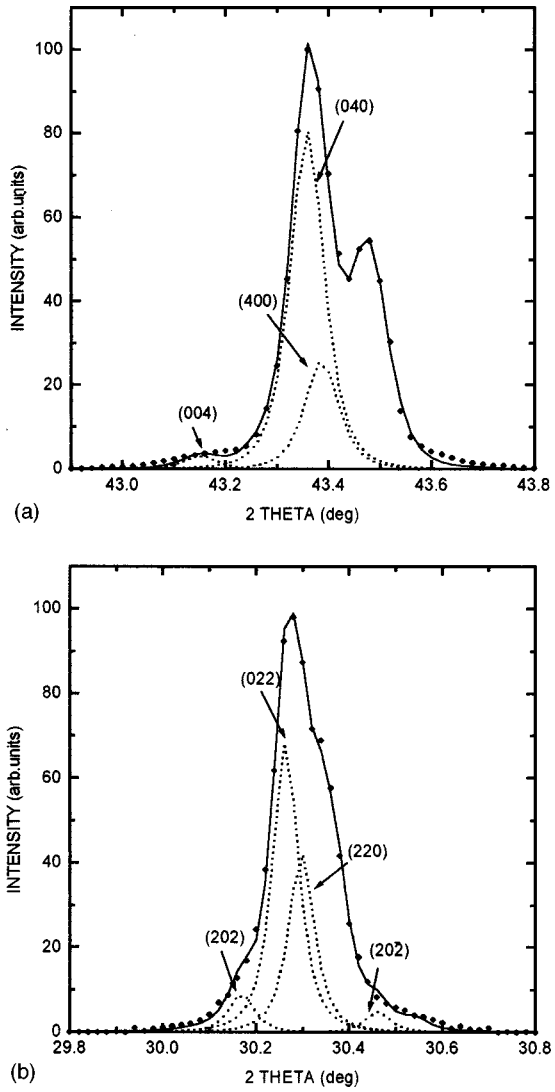

FIG. 1. Splitting of the {400} and {220} diffraction lines at $T = 12$ K characteristic for monoclinic distortion. (a): {400}, (b): {220}.

Raman spectra were recorded with a Dilor Z-24 spectrometer single-channel triple monochromator coupled with a Coherent 90-3 laser beam. The 488 nm excitation line was mainly used with an incident power of 500 mW. Low-temperature measurements were performed from 30 up to 300 K using a Leybold cryogenerator.

VIBRATIONAL ANALYSIS

The symmetries of the vibrational normal modes are calculated on the basis of usual group theory analysis (method of site symmetry) at the center of different Brillouin zones according to the previously given sequence for the phase transitions. Table I summarizes the irreducible representations associated with the motions of three different atoms in the different phases. The Mn^{2+} ion was chosen as the origin of the cubic cell for all calculations since the rotating fluorine octahedron is centered on this ion. Then no Raman line is expected in the ideal cubic perovskite phase while seven Raman lines are predicted to appear in the tetragonal phase $(A_{1g}\oplus B_{1g}\oplus 2B_{2g}\oplus 3E_g)$. Twenty-four Raman peaks are expected in case of a low-temperature orthorhombic symmetry $(7A_g\oplus 5B_{1g}\oplus 7B_{2g}\oplus 5B_{3g})$ and also 24 in case of a monoclinic symmetry $(14A_g\oplus 10B_g)$. So, this group theory analysis shows that the two possible low-temperature phases cannot be identified considering only the number of active Raman lines. However, it can be noticed that despite the fact that the two possible low-temperature structures have an equivalent number of active Raman lines, the *I*4/*mcm* tetragonal to *Pnma* orthorhombic transition is not associated with group-subgroup relation, as opposite to the *I*4/*mcm* to $P2_1/m$ monoclinic one. The Raman spectra and the behavior of the sample have to reflect this difference.

In order to index the Raman spectra, lattice dynamics in the cubic phase of $KMnF_3$ was approached using a rigid-ion model.[30,31] Theoretical calculations of the vibrational eigenfrequencies were performed at the $\Gamma_C(0,0,0)$, $R_C(0.5,0.5,0.5)$, $M_C(0.5,0,0.5)$, and $X_C(0,0.5,0)$ points of the cubic Brillouin zone, which gives rise to the Raman active lines in the lowest temperature symmetries. This model is classically defined by eight adjustable parameters: (i) the ionic effective charges Z^*_K, Z^*_{Mn} (Z^*_F is given by the charge neutrality condition: $Z^*_K+Z^*_{Mn}+3Z^*_F=0$), (ii) the longitudinal A_i and transverse B_i short-range force constants between first neighbors, defined by the second derivative of the Born-Mayer interaction potential.[31] The subscripts $i=1,2,3$ are re-

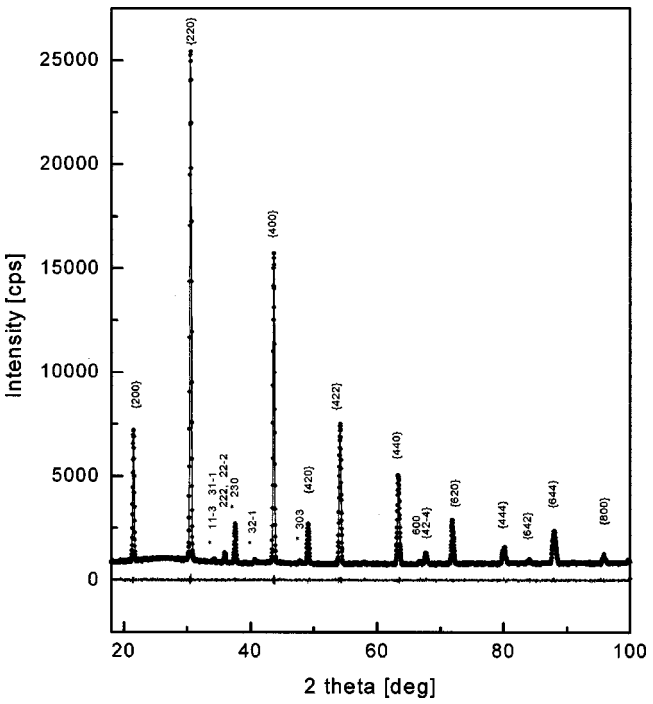

FIG. 2. X-ray-diffraction pattern: observed, calculated, and difference profiles at $T=12$ K. Lines of super structure are marked by stars (*).

TABLE III. Structural parameters for $KMnF_3$ at $T=12$ K. a_m, b_m, c_m: parameters of the monoclinic cell described in $B2_1/m$. a_p, b_p, c_p: pseudocubic parameters $a_m=2a_p$, $b_m=2b_p$, $c_m=2c_p$.

Space group: $B2_1/m$, $Z=8$
Lattice parameters:
$a_m=8.3281(4)$ Å $b_m=8.3392(4)$ Å $c_m=8.3695(3)$ Å $\beta=89.72°$
$a_p=4.1641(4)$ Å $b_p=4.1696(4)$ Å $c_p=4.1848(3)$ Å $\beta=89.72(1)°$.
Rotation angles of the MnF_6 octahedra along pseudocubic axes:
$\alpha=3.95°$, $\beta=4.32°$, $\gamma=4.08°$.

Atomic positions:

Atom	Site	x	y	z	$B[A^2]$
K(1)	4*e*	0.2518(5)	1/4	0.2474(3)	1.83(4)
K(2)	4e	0.2930(3)	1/4	0.6888(3)	1.83(4)
Mn(1)	4*a*	0	0	0	0.62(3)
Mn(2)	4*c*	0	0	1/2	0.62(3)
F(1)	4*e*	0.0604(8)	1/4	0.0631(8)	2.82(5)
F(2)	4*e*	0.0637(6)	1/4	0.5144(7)	2.82(5)
F(3)	8*f*	0.2393(7)	0.0091(5)	0.0208(7)	2.82(5)
F(4)	8*f*	0.0489(5)	0.0147(9)	0.2794(6)	2.82(5)

$R=0.052$
$R_B=0.085$ Durbin-Watson statistic parameter=0.85

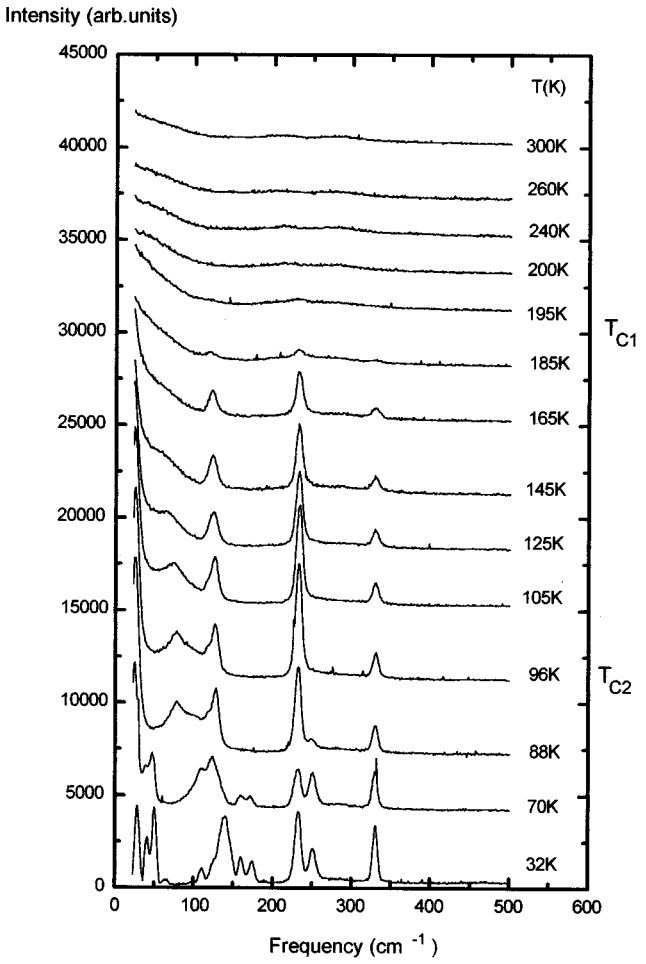

FIG. 3. Raman spectra of $KMnF_3$ versus temperature.

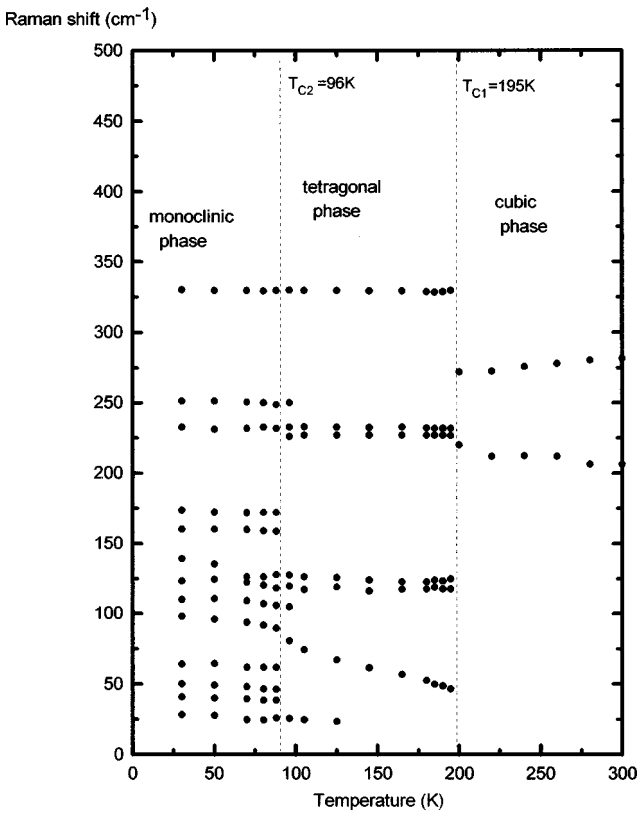

FIG. 4. Evolution of Raman frequencies versus temperature.

spectively related to the K-F, Mn-F, and F-F interactions. The set of parameters used for calculations was estimated by applying on the experimental data of Gesi *et al.*[32] This set of parameters and the calculated frequencies of the eigenmodes at the Γ_C, R_C, X_C, and M_C points of the cubic Brillouin zone are summarized in Table II.

RESULTS AND DISCUSSION

The space-group determination of the low-temperature phase (below 91 K) was achieved by considering the Glazer's structural description[11] for distorted perovskites by rotation of octahedra around their cubic axes. In these perovskites, the distortion type and the tilt system can be normally deduced from the splitting occurring on the $(h00)$, $(hh0)$, (hhh), or (hkk) main intense cubic reflections. However, in order to establish unambiguously the space group, we also collected a pattern over a wider angular range and a full powder-diffraction diagram was used for structural Rietveld refinements (320 collected reflections were refined with the FULLPROF program[33]). Moreover, the angles of rotation of the MnF_6 octahedra, as well as the displacement of the atoms from their ideal cubic positions were obtained using the POTATO program.[34]

The distinction between the two tilt systems $a^-b^+a^-$ (orthorhombic-*Pnma*) and $a^-b^+c^-$ (monoclinic-$P2_1/m$) can be noticed as illustrated in Fig. 1 by a characteristic splitting of the {400} and {220} diffraction lines ($T=12$ K). In case of the $a^-b^+a^-$ distortion, involving two equal tilt angles, the {400} and {220} diffraction lines have to be respectively split in two and three components, instead of three and four, respectively, in case of three different tilt angles associated to the $a^-b^+c^-$ monoclinic system. Figure 1 shows that the splitting of the lines observed is characteristic for the $P2_1/m$ monoclinic symmetry. It should be noted that there is a difference in the description of the low-temperature deformation between $RbCaF_3$ and $KMnF_3$. In case of the former, in monoclinic phase certain values of the rotation angles of CaF_6 octahedra along $[100]_c$ and $[001]_c$ axes are the same ($\alpha \approx \gamma$) and this type of distortion is described as $a^-b^+a^-$ (*Pnma*). In the case of $KMnF_3$, as previously evidenced, the characteristic splitting of the main diffraction lines has shown that the rotation angles are slightly different ($\alpha=3.95°$, $\gamma=4.08°$). This small difference in the values of the rotation angles of fluorine octahedra causes considerable consequences in the description of the symmetry of low-temperature phases and the unit cells are described now by space groups showing different symmetries. So, in the case of the $a^-b^+c^-$-type distortion, the adequate double unit cell of $2a_p \times 2b_p \times 2c_p$ dimensions (where a_p, b_p, and c_p—the parameters of distorted pseudocubic unit cell) is monoclinic with a $B2_1/m$ space group (which is equivalent to $P2_1/m$). In case of a distortion which originates as a result of freezing of the tilts of octahedra with $a^-b^+a^-$ system, a unit cell of $a_p\sqrt{2} \times 2b_p \times a_p\sqrt{2}$ dimensions is orthorhombic with *Pnma* space group ($RbCaF_3$).[11] The refinement of the full diffraction pattern confirms the monoclinic symmetry observed for $KMnF_3$ below 91 K. Figure 2 illustrates the experimental

TABLE IV. Assignment of active Raman lines in the three phases of $KMnF_3$. Comparison is performed with isostructural $NaMnF_3$ (Ref. 37), $KCaF_3$ (Ref. 38) and $RbCaF_3$ (Ref. 35). Because these three last compounds in their low-temperature phase are orthorhombic (*Pnma*) a corresponding assignment in this symmetry is given, n.o. are nonobserved modes. Symbols ↕ or ↕→ indicate the impossibility to differentiate unambiguously the assignment of a Raman mode, respectively between 2 or 3 eigensymmetries.

Cubic modes	$KMnF_3$ Rigid-ion model [cm^{-1}]	Tetragonal modes	$KMnF_3$ T=150K [cm^{-1}] (This work)	$RbCaF_3$ T=50K [cm^{-1}]	$KMnF_3$ T=32K [cm^{-1}] (This work)	Mono-clinic modes	Ortho-rhombic modes	$RbCaF_3$ T=15K [cm^{-1}]	$NaMnF_3$ T=40K [cm^{-1}]	$KCaF_3$ T=40K [cm^{-1}]
R'_{15}	23.1	E_g	**n.o.**	n.o.	**28.5**	B_g	B_{1g}	31.0	n.o	66.0
					40.9	A_g	B_{2g}	36.0	n.o	96.0
		A_{1g}	**61.2**	82.0	**98.3**	A_g	A_g	84.4	183.0	144.0
M_2	24.1	X_4	**i**	i	**50.4**	A_g	A_g	44.0	250.0	n.o.
X_5	98.2	X_4	**i**	i	↑ **64.6**	A_g	A_g	n.o.	88.0	n.o.
		X_3	**i**	i	↓ **n.o.**	A_g	B_{2g}	n.o.	140.0	n.o.
R'_{25}	106.7	E_g	**120.3**	74.0	↕ **110.4**	A_g	A_g	↑75.6	143.0	↑ n.o.
					→**123.5**	B_g	B_{3g}	↓ 79.7	96.0	86.0
		B_{2g}	**126.2**	87.7	↓ **139.2**	A_g	B_{2g}	n.o.	155.0	↓105.0
X_1	126.89	X_1	**i**	i	**n.o.**	B_g	B_{1g}	94.9	182.0	n.o.
M_5	176.0	X_1	**i**	i	↑ **n.o.**	B_g	B_{1g}	↑127.8	160.0	↑113.0
		X_2	**i**	i	↓ **160.4**	B_g	B_{3g}	↓150.8	n.o.	↓147.0
X_5	185.9	X_4	**i**	i	↑ **173.7**	A_g	A_g	↑140.0	212.0	139.0
		X_3	**i**	i	↓ **187.5**	A_g	B_{2g}	↓ n.o.	201.0	184.0
R'_{25}	265.1	E_g	**227.0**	202.0	↑ **n..o.**	A_g	B_{2g}	↑200.4	n.o.	↑221.0
					→**251.3**	B_g	B_{3g}	↓215.9	226.0	195.0
		B_{2g}	**232.0**	210.0	↓ **232.5**	A_g	A_g	207.6	270.0	↓228.0
M_4	265.9	X_4	**i**	i	**n.o.**	A_g	B_{2g}	233.5	293.0	251.0
R_{12}	317.0	B_{1g}	**330.0**	364.0	↕ **330.3**	B_g	B_{1g}	364.0	312.0	↑347.0
		A_{2g}	**i**	i	↓ **n.o.**	B_g	B_{3g}	n.o.	302.0	↓ n.o.
M_3	317.1	X_3	**i**	i	**n.o.**	A_g	A_g	n.o.	319.0	n.o.
X_1	373.8	X_1	**i**	i	**n.o.**	B_g	B_{1g}	385.0	426	n.o.
M_1	413.1	X_3	**i**	i	**n.o.**	A_g	B_{2g}	n.o.	n.o.	n.o.
R_1	448.5	A_{2g}	**i**	i	**n.o.**	B_g	B_{3g}	418	n.o.	415.0

diagram at $T=12$ K and compares it to the calculated one in the framework of $P2_1/m$ space group. Table III summarizes the structural parameters refined at the same temperature.

From the Raman-scattering results, the transition located at $T_{C2}=91$ K is characterized by the appearance of three sharp low-frequency modes, with slight temperature dependence, below T_{C2}, as evidenced by Fig. 3 where Raman spectra versus temperature are displayed. It could be also noted in Fig. 4 where the temperature evolution of all Raman frequencies is shown. These three modes, respectively, located at 41, 50, and 64.5 cm^{-1} at $T=32$ K, do not possess a soft-mode behavior. Together with the temperature decrease, a sudden appearance of several low-frequency Raman lines (with A_g symmetries) was observed. Their full width at half maximum (about 6 cm^{-1}) is smaller than typical values (close to 10 cm^{-1}) for the other lines in the $KMnF_3$ spectra. These several lines coming from the R'_{15} and M_2 cubic modes of the cubic phase illustrate unambiguously the first-

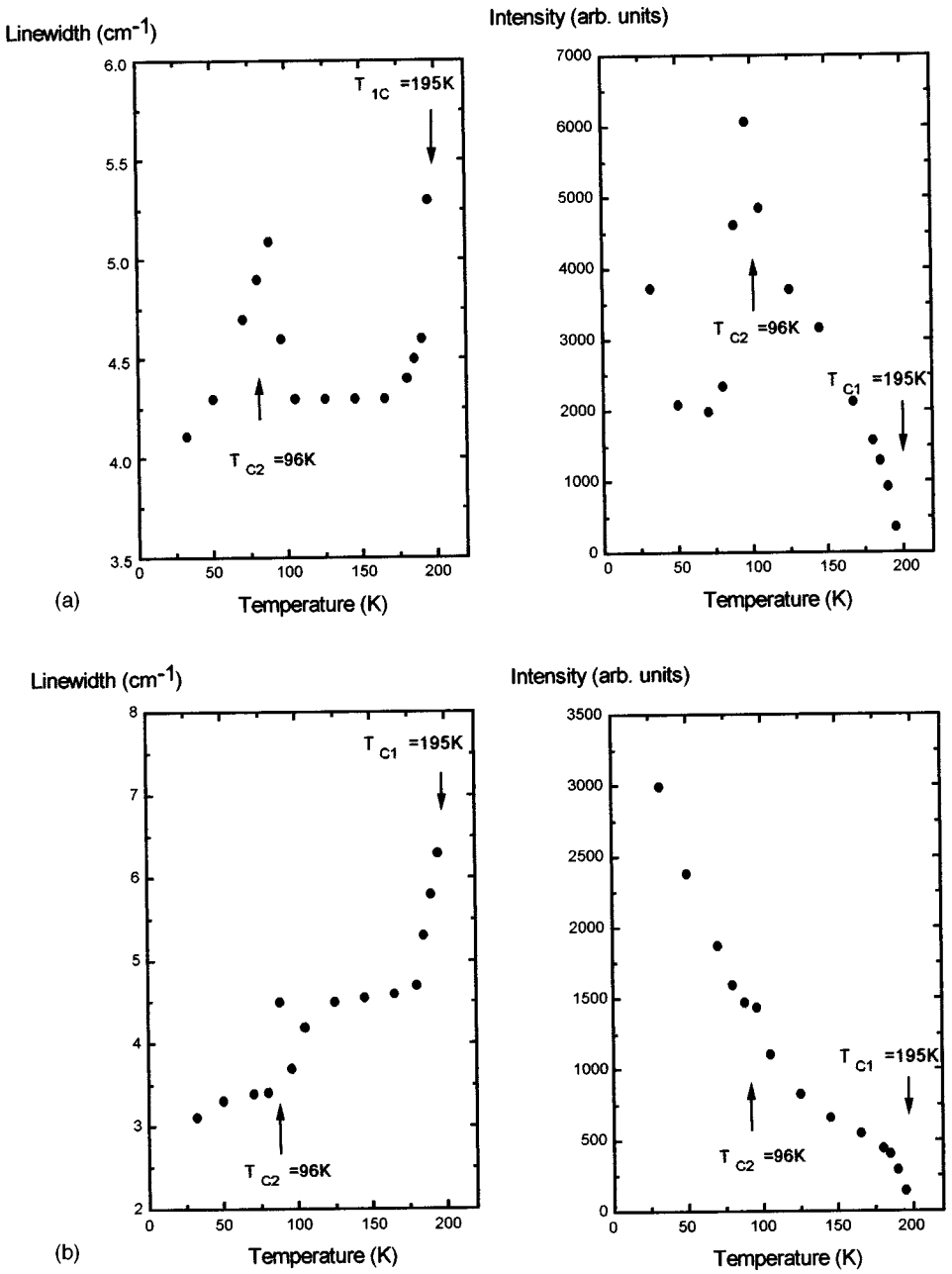

FIG. 5. Linewidths and Raman integrated intensities for two hard modes of $KMnF_3$. (a) Raman peak located at 232 cm^{-1} at $T=150$ K of B_{2g} tetragonal symmetry; (b) Raman peak located at 330 cm^{-1} at $T=150$ K of B_{1g} tetragonal symmetry.

order character of this low-temperature phase transition, contrary to the assertion of Hidaka *et al.*[14] who attributes a second-order character to this transition. Furthermore, except for the behavior of the previously discussed low-frequency modes, the continuous character of the evolution of Raman spectra can be noted in Fig. 3, especially performing successive temperature cycles on the sample, do not affect in any manner the crystal, contrary to the ''violent'' $I4/mcm$ to *Pnma* first-order transition which occurs in $RbCaF_3$ at $T_{C2}=31.5$ K.[35,36] This significant difference between the two samples is an indication for the existence of a group-subgroup relation between the tetragonal phase and the lowest temperature one in $KMnF_3$. Actually, the $P2_1/m$ (or the equivalent $B2_1/m$) monoclinic space group proposed (at the light of our x-ray-diffraction work) to describe the low-temperature structure of $KMnF_3$, is a subgroup of the tetragonal $I4/mcm$ space group, in opposition to the orthorhombic *Pnma* space group. This indication also argues with a monoclinic symmetry below 91 K as obtained by the x-ray-diffraction analysis. Therefore the sequence of SPT adopted in $KMnF_3$ in terms of octahedra rotations seems to be as follows:

$$\underset{\text{cubic}}{a^0a^0a^0} \xrightarrow{186\ \text{K}} \underset{\text{tetragonal}}{a^0a^0c^-} \xrightarrow{91\ \text{K}} \underset{\text{monoclinic.}}{a^-b^+c^-}$$

As previously indicated, the Raman experiments were performed in the temperature range 30–300 K. The selection rules for Raman-scattering active modes are of course very helpful in order to index the Raman spectra but unfortu-

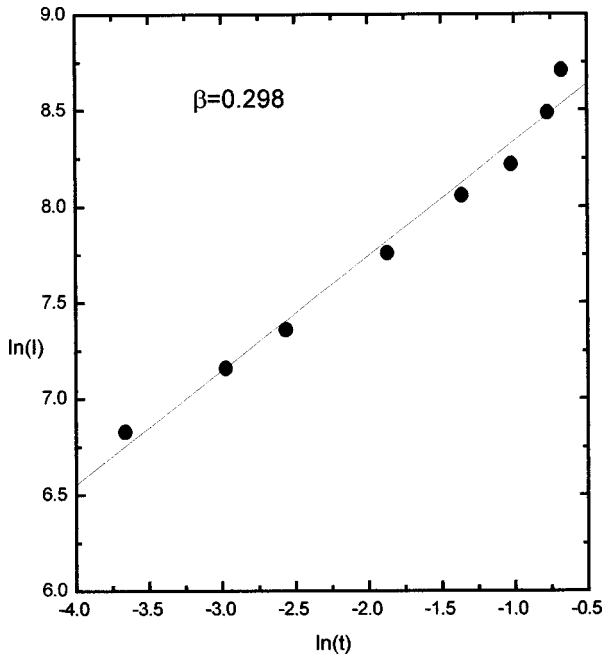

FIG. 6. Logarithmic representation of Raman integrated intensity versus temperature for the B_{2g} mode, located at 232 cm^{-1} at $T=150$ K.

nately, $KMnF_3$, as many other perovskite-type compounds, tends to transform to a polydomain character. As a result, all spectral lines which appear in the polarized Raman spectra, despite the particular scattering configurations and the selection rules, become inoperative. So, the correct assignment of the Raman spectra in each phase was only possible using the lattice dynamics calculations. Actually, the eigenfrequencies predicted by the model can be followed with the compatibility relations between all the phases, previously established in the quasi-isostructural $RbCaF_3$,[35] assuming that modes which are not involved in the transition are temperature independent. Additionally, comparison to the Raman results obtained for structurally identical compounds $NaMnF_3$,[37] $KCaF_3$,[38] and also $RbCaF_3$ (Ref. 35) confirmed the proposed assignment. So, the Raman spectra of $KMnF_3$ were attributed in its three phases. The final results are listed in Table IV.

The first transition which occurs at $T_{C1}=186$ K is confirmed by the softening of two tetragonal modes (of E_g and A_{1g} symmetries) and the disappearance of the tetragonal Raman peaks when cubic symmetry occurs (see Fig. 3). The results obtained for the tetragonal phase are fully consistent with the literature.[17–20] Note that in this phase, as listed in Table IV, only six active Raman lines were observed among the seven which were predicted from the group theory calculations for tetragonal symmetry. Particular attention was paid to modes which are not directly involved in the SPT and which are usually named ''hard Raman modes'' because their frequencies are temperature independent. These modes are usually well resolved so that their linewidth and intensity evolution versus temperature can be easily established. It was shown[35] that intensity of hard Raman modes can be related to the power law

$$I \propto t^{2\beta},$$

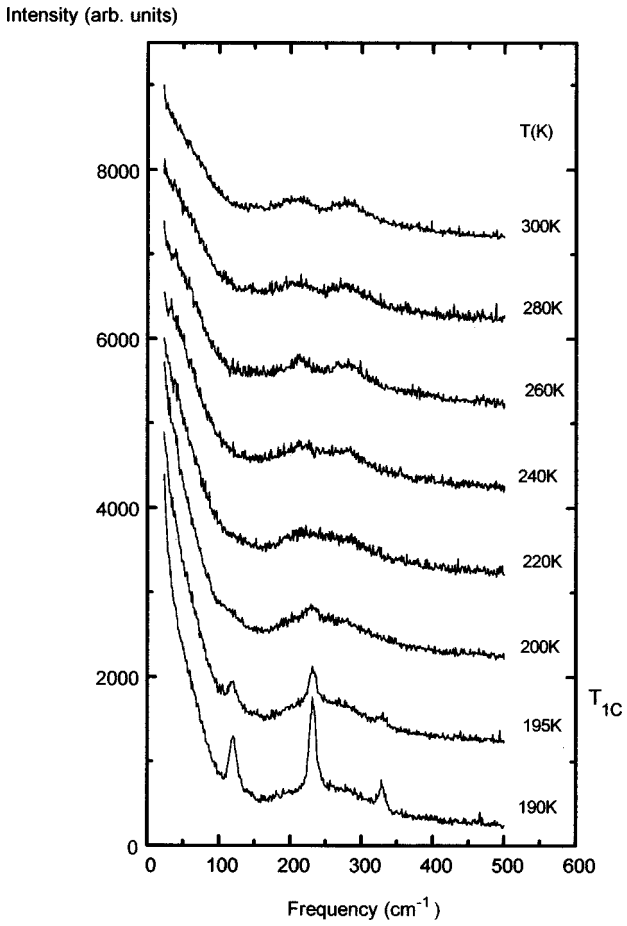

FIG. 7. Detailed evolution of the $KMnF_3$ Raman spectra versus temperature in the cubic phase.

where β is the critical exponent for the order parameter and $t=(T_{c1}-T)/T_{c1}$—the reduced temperature. According to the phenomenological Landau theory, β is expected to be equal to 0.5, while in the three-dimensional microscopic Ising model β was found to be equal to 0.31. Experimentally, $0.25 \leqslant \beta \leqslant 0.5$ (see, for instance, the three review papers given in Ref. 39). We especially focused on hard modes located at 232 cm^{-1} (tetragonal B_{2g} mode at $T=150$ K) and 330 cm^{-1} (tetragonal B_{1g} mode at $T=150$ K). The lines were fitted with a Gaussian shape to obtain position, intensity and half-width values. Figure 5 shows a plot of intensity and half-width versus temperature for these two hard modes, and it is shown that they are very sensitive to the symmetry changes. For the most intense hard mode which originates from the R'_{25} cubic mode located at 232 cm^{-1}, the critical exponent was found to be $\beta=0.298$ (see Fig. 6). Similar results ($\beta=0.237$) were obtained for mode coming from R_{12} cubic mode and located at 330 cm^{-1}.

According to selection rules, no Raman line is expected in the centrosymmetric cubic phase (see Table I), however, two very broad bands, located at 211 and 278 cm^{-1} at $T=260$ K, can be clearly observed above the T_{C1}—the temperature of the cubic to tetragonal phase transition. As shown in Fig. 7 where a detailed evolution versus temperature of the Raman spectra is displayed from 180–300 K, this unusual Raman activity in the cubic phase starts in the tetragonal phase, constituting broad bands ''under'' the tetragonal

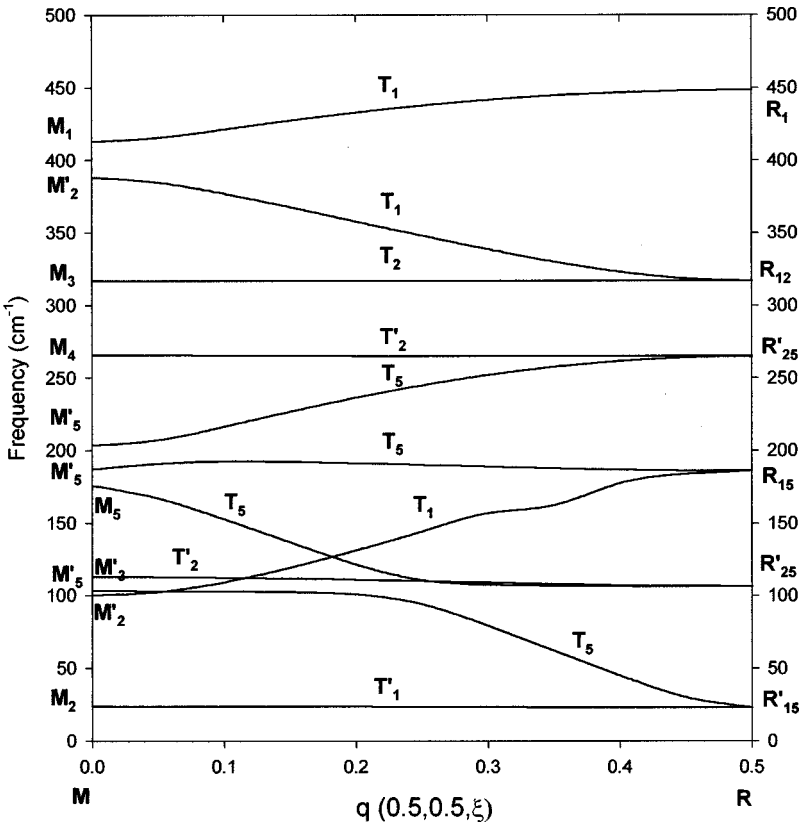

FIG. 8. Calculated phonon spectrum along the R-$M(0.5,0.5,\xi)$ direction, obtained from parameters listed in Table II, and fitted on experimental data of Ref. 32.

peaks. Moreover, with increasing temperature from room temperature to T_{C1}, the peak located at 211 cm^{-1} does not move in frequency (only a slight classical decrease) whereas the second one, at 278 cm^{-1}, increases significantly. The main question is then: what is the physical origin of these two unusual broads bands?

First, the existence of these bands cannot be associated with persistence of tetragonal hard modes. Together with careful attention to Raman spectra around T_{C1}, it appears that both cubic peaks and some tetragonal modes coexist at a 15 K temperature range, which suggests only a weak hysteresis and phase coexistence in this small temperature range.

Additionally, it seems that it cannot be due to pure second-order Raman spectrum, as it occurs rather commonly in oxygen perovskites (see for instance Refs. 40–42). Actually, the low polarizability of fluorides, and especially $KMnF_3$ as compared to $RbCaF_3$, $KCaF_3$, and $RbMnF_3$ where no such Raman signal has been detected yet, prevents attribution of this intensity to such origin. However, we have to be very careful about this analysis; actually, the difference between pure second-order and first-order Raman signal (induced for instance by disorder), especially in systems exhibiting structural instabilities, has not been fully understood until now. Especially the two mechanisms can be invoked when disorder leads to a nonpredicted Raman intensity by folding of phonons branches, which are able to combine between each other, in a second-order process to give rise to such a signal. The value of the full width at half maximum (FWHM) of the two cubic bands, which is about 47.5 cm^{-1} (for the mode located at 211 cm^{-1}) and 60.4 cm^{-1} (for mode located at 278 cm^{-1}), is large as compared to typical values of 10 cm^{-1} that the tetragonal Raman modes have. It seems to indicate that the origin of these bands could be related to the existence of structural disorder.

Considering Fig. 8, which shows the phonon spectrum along the R-M direction calculated on the basis of the parameters given in Table II, it seems to be possible to propose an explanation of these two bands. The existence of numerous quasiflat branches in this phonon spectrum along this R-M direction, involved in the instability, could then give to a more probable second-order Raman activity by combinations between frequencies of these branches. This activity would be also connected with the existence of structural disorder above T_{C1}. Especially, the observed band located at 211 cm^{-1} could be due to modes coming from the R'_{25}-M'_3 (T'_2) phonon branch, calculated at $\sim$105 cm^{-1} (see Table II and Fig. 8) which evidently could give rise to a second-order Raman band located at twice frequency, that is $\sim$210 cm^{-1}. This process involves only temperature-independent modes as it was experimentally shown. The second broadband at 278 cm^{-1}, which increases with temperature, probably involves the quasiflat soft branch R'_{15}-M_2 (T'_1) combined with another quasiflat branches. From our calculations the existence of such branches close to $\sim$255 cm^{-1} could be due to T'_2: R'_{25}-M_4 at 265 cm^{-1} and to a part of T_5: R'_{25}-M'_5 at $\sim$245 cm^{-1}. It seems then that this second broadband could be assigned to the combination of $T'_1+(T'_2,T_5)$. Then the frequency evolution of the soft branch R'_{15}-M_2 versus temperature can be deduced from the evolution of the broadband located at 278 cm^{-1} at $T=260$ K, assuming that the (T'_2,T_5) branches are temperature independent and located, as calcu-

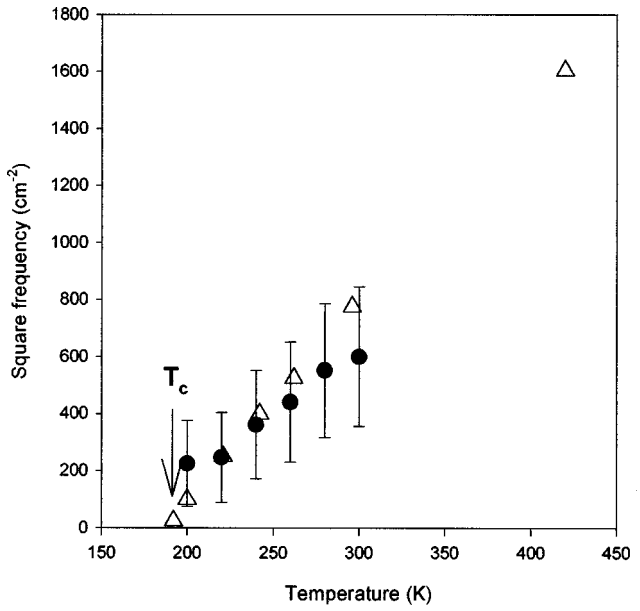

FIG. 9. R'_{15} soft-mode evolution versus temperature in $KMnF_3$. Comparison between data extracted from Raman scattering (this work: full circles) to inelastic neutron scattering of Gesi *et al.* (open triangles taken from Ref. 32).

lated by lattice dynamics, at 255 cm^{-1}. A soft branch located at a corner of the Brillouin zone can be followed versus temperature only from Raman-scattering data in this kind of perovskite compound. So, Fig. 9 displays the evolution of the R'_{15} soft mode versus temperature, deduced from the Raman signal occurring in the cubic phase. It is especially noteworthy that these results are fully consistent with the neutron-scattering measurements of Gesi *et al.*;[32] in the limit of precision of our estimation. Beyond this ''exotic'' characteristic of Raman spectra, the observation of such signal related to the modes responsible for the phase transition seems to indicate the existence of structural disorder far above the transition temperature as predicted by theoretical models[23,24] and in agreement with recent XAFS experiments in oxygen perovskites.[25–27] It should be noted that these two unusual bands were previously mentioned in the work of Lockwood and Torrie[18] and also by Bruce, Taylor, and Murray;[21] however, their proposed assignment to particular combination of zone-boundary modes seems to be rather improbable.

CONCLUSION

The reinvestigation of the structural and vibrational behavior of the archetype $KMnF_3$ perovskite allows to remove the structural ambiguities still persisting in this compound, and suggests that the low-temperature symmetry is monoclinic associated with the $P2_1/m$ space group. Furthermore, the tetragonal to cubic phase transition was interpreted in terms of hard Raman modes and disorder, the evidence of which is given by an unusual Raman activity. So it could be suggested that far above $T_{C1}(\sim 100\,K)$, an intermediate disordered phase with cubic average symmetry could exist and could constitute the final stage of precursor effects shown with the phase coexistence on a 15 K temperature range. Additionally, the dependence of the integrated intensity of hard tetragonal modes versus the tilt angle of octahedra could indicate that this disordered phase starts with rotations around *c* cubic axis of the entire regions in the crystal, while other regions remain cubic. We have to underline that precursor effects which are enhanced in case of $KMnF_3$, as compared to other fluoroperovskites, induce this exceptional second-order activity in the cubic phase associated with a partial folding of the Brillouin zone.

Moreover, the experimental evidence of such disorder, exhibited here on the basis of Raman scattering, have to be related to the growth of a quasielastic scattering, usually named central peak in neutron-scattering experiments, the origin of which (either intrinsic or due to impurities in the host crystal) was conflicting during a long time.[32–43] Finally, even if these Raman results do not constitute unambiguous proof for the existence of such disordered phase, this understanding of the antiferrodistortive structural transitions merges with recent results (see, for instance, Yacoby and Stern,[27] and numerous references therein) in perovskites which showed that low-temperature local distortions remain considerably above T_C, as opposed to a pure displacive mechanism vision.

ACKNOWLEDGMENTS

This work is a part of the scientific program between the University of Silesia and the Université du Maine. The authors would like to thank the French Embassy in Warsaw for financial support. We are also fully indebted to Professor M. Rousseau for his invaluable discussions. The help of G. Ripault in Raman-scattering technical assistance and Eng. G. Niesseron for crystal growth is also acknowledged.

*Author to whom correspondence should be addressed.

[1] G. Shirane and Y. Yamada, Phys. Rev. **177**, 858 (1969).
[2] P. A. Fleury, J. F. Scott, and J. M. Worlock, Phys. Rev. Lett. **21**, 16 (1968).
[3] H. A. Klassens, P. Zalm, and F. O. Huysman, Philips Res. Rep. **8**, 441 (1953); see also R. L. Martin, R. S. Nyholm, and N. C. Stephenson, Chem. Ind. 83 (1956).
[4] A. Okasaki, Y. Suemune, and T. Fuchikami, J. Phys. Soc. Jpn. **14**, 1823 (1959).
[5] O. Beckman and K. Knox, Phys. Rev. **121**, 376 (1961).
[6] M. A. Vinnik and L. N. Selezneva, Kristallografiya **14**, 1068 (1969) [Sov. Phys. Crystallogr. **14**, 928 (1970)].
[7] V. J. Minkiewicz and G. Shirane, J. Phys. Soc. Jpn. **26**, 674 (1970).
[8] V. J. Minkiewicz, Y. Fun, and Y. Yamada, J. Phys. Soc. Jpn. **28**, 443 (1970).
[9] U. Nicholls and R. A. Cowley, J. Phys. C **20**, 3417 (1987).
[10] A. Gibaud, S. M. Shapiro, J. Nouet, and H. You, Phys. Rev. B **44**, 2437 (1991).
[11] A. M. Glazer, Acta Crystallogr., Sect. A: Cryst. Phys., Diffr., Theor. Gen. Crystallogr. **A31**, 756 (1975); Acta Crystallogr., Sect. B: Struct. Crystallogr. Cryst. Chem. **B28**, 3384 (1972).
[12] G. Shirane, V. J. Minkiewicz, and A. Linz, Solid State Commun. **8**, 1941 (1970).
[13] V. G. Khlyustov, I. N. Flerov, A. T. Silin, and A. N. Sal'nikov, Fiz. Tverd. Tela (Leningrad) **14**, 175 (1972) [Sov. Phys. Solid State **14**, 139 (1972)].
[14] M. Hidaka, M. Ohama, A. Okasaki, H. Sakashita, and S. Ya-

makawa, Solid State Commun. **16**, 1121 (1975).
[15] A. Ratuszna and A. M. Glazer, Phase Transit. **12**, 347 (1988).
[16] A. Ratuszna and K. Majewska, Powder Diffr. **5**, 41 (1990).
[17] Yu. A. Popkov, V. V. Eremenko, and V. I. Fomin, Fiz. Tverd. Tela (Leningrad) **13**, 2028 (1972) [Sov. Phys. Solid State **13**, 1701 (1971)].
[18] D. J. Lockwood and B. H. Torrie, J. Phys. C **7**, 2729 (1974).
[19] B. H. Torrie and D. J. Lockwood, Ferroelectrics **8**, 583 (1974).
[20] D. J. Lockwood and B. H. Torrie, in *Anharmonic Lattices, Struct. Transitions Melting, NATO Advanced Study Institute, Series E: Applied Sciences* (Kluwer, Dordrecht-Netherland, 1974), p. 147.
[21] A. D. Bruce, W. Taylor, and A. F. Murray, J. Phys. C **13**, 483 (1980).
[22] Yu. A. Popkov and V. I. Fomin, Zh. Eksp. Teor. Fiz., Pis'ma Red. **11**, 394 (1970) [JETP Lett. **11**, 264 (1970)].
[23] A. Bulou, M. Rousseau, and J. Nouet, Ferroelectrics **104**, 373 (1990).
[24] W. C. Kerr and A. R. Bishop, Phys. Rev. B **34**, 6295 (1986).
[25] B. Rechav, N. Sicron, Y. Yacoby, B. Ravel, M. Newville, and E. A. Stern, Physica C **209**, 55 (1993).
[26] E. A. Stern and Y. Yacoby, J. Phys. Chem. Solids **57**, 1449 (1996).
[27] Y. Yacoby and E. A. Stern, Comments Condens. Matter Phys. **18**, 1 (1996).
[28] M. Rousseau, Ph. Daniel, J. Toulouse, and B. Hennion, Physica B **234-236**, 139 (1997).
[29] J. Nouet, Proc. SPIE **3178** (1997).
[30] R. A. Cowley, Phys. Rev. A **134**, 981 (1964).
[31] M. Rousseau, J. Nouet, and R. Almairac, J. Phys. (France) **38**, 1423 (1977).
[32] K. Gesi, J. D. Axe, G. Shirane, and A. Linz, Phys. Rev. B **5**, 1933 (1972).
[33] J. Rodriguez-Carvajal, FULLPROF program (1972).
[34] P. Woodward, Acta Crystallogr., Sect. B: Struct. Sci. **B53**, 32 (1997).
[35] Ph. Daniel, M. Rousseau, and J. Toulouse, Phys. Rev. B **55**, 6222 (1997).
[36] F. A. Modine, E. Sonder, W. P. Unruh, C. B. Finch, and R. D. Westbrook, Phys. Rev. B **10**, 1623 (1974).
[37] Ph. Daniel, M. Rousseau, A. Désert, A. Ratuszna, and F. Ganot, Phys. Rev. B **51**, 12 337 (1995).
[38] Ph. Daniel, M. Rousseau, and J. Toulouse, Phys. Status Solidi B **203**, 327 (1997).
[39] R. A. Cowley, Adv. Phys. **29**, 1 (1980); A. D. Bruce, *ibid.* **29**, 111 (1980); A. D. Bruce and R. A. Cowley, *ibid.* **29**, 219 (1980).
[40] G. E. Kugel, H. Mesli, M. D. Fontana, and D. Rytz, Phys. Rev. B **37**, 5619 (1988).
[41] A. Grzechnik, H. W. Wolf, and P. F. McMillan, J. Raman Spectrosc. **28**, 885 (1997).
[42] G. Kugel, I. Jankowska-Sumara, K. Roleder, and J. Dec, J. Korean Phys. Soc. **32**, S581 (1998).
[43] S. M. Shapiro, J. D. Axe, G. Shirane, and T. Riste, Phys. Rev. B **6**, 4332 (1972).